# Hot-Electron Behavior in Germanium under the Influence of a Magnetic Field*

LOUIS GOLD†
*Lincoln Laboratory, Massachusetts Institute of Technology, Lexington, Massachusetts*
(Received June 26, 1958; revised manuscript received December 15, 1958)

The theory of the hot-electron problem in many-valley semiconductors based upon the individual ellipsoidal energy surface model is extended for germanium to the circumstance of a superposed magnetic field **B**. A first approach, ignoring collisional effects, allows ready delineation of the electron orbits; directional energy gain is evaluated for $\mathbf{E}_{100}$ and $\mathbf{E}_{110}$ with **B** rotated in longitudinal and transverse orientations. The anisotropy is found to be quite marked (decidedly stronger than for $\mathbf{B}=0$), with the longitudinal arrangement more effective than the transverse one. The introduction of scattering considerably complicates the analysis and here consideration is given to the effective ratio $b$ of Larmor to scattering frequency. In the limit $b\rightarrow\infty$ and the scattering decidedly anisotropic, transverse energy gain vanishes; whereas in the longitudinal alignment, the energy gain becomes extremely anisotropic. The shift in the optimal energy gain direction(s) is noted for selected combinations of **E** and **B** and comparisons made with the case $\mathbf{B}=0$. As $b\rightarrow 0$, the anisotropy diminishes; detailed calculations have been performed for $b=1$, 0.1, and $\infty$ for the limiting cases of isotropic and strongly anisotropic scattering.

## INTRODUCTION

In a previous work, the hot-electron problem in many-valley semiconductors like germanium and silicon was especially examined from the point of view of the nature of the anisotropy.[1] The present article considers the same question in the more complicated circumstance of a superposed magnetic field.

Experimental observations of breakdown in polycrystalline germanium at low temperatures (where presumably impurity ionization is involved) reveal that a magnetic field decidedly increases the threshold electric field.[2] There evidently has been no reported research on the phenomenon in oriented single crystals. It is the purpose of this paper to deal primarily with the anisotropy factor in the temperature region of interest where the individual ellipsoidal energy surfaces make their separate contributions to the breakdown process. The contribution of the external magnetic field may be characterized in terms of the ratio of Larmor to collision frequency. The directional nature of the breakdown will embody this parameter, allowing also for possible anisotropic scattering.

The limiting case of zero scattering will be described for purposes of comparison with the nonconservative situation and for delineation of the ideal cyclotron orbits that may occur in a tensor-mass medium. Actually, this case is also representative of the situation where the collision time is much longer than the oscillation period.

## CONSERVATIVE EQUATIONS OF MOTION FOR MANY-VALLEY ELECTRONS

In considering the component from the basic vector equation

$$\frac{d}{dt}(\mathfrak{m}\cdot\mathbf{v})=q\mathbf{E}+q\mathbf{v}\times\mathbf{B}, \tag{1}$$

it is convenient to choose Cartesian coordinates with the $z$ axis always along the direction of the magnetic field **B** and the components of the electric field **E** completing the orthogonal system. Accordingly, the mass tensor $\mathfrak{m}$ in the cubic reference frame will need to be transformed to these axes. Thus, the components of (1) become, after some reduction,

$$\begin{aligned}
M_1\dot{v}_x+M_2\dot{v}_y&=-\frac{m_{13}}{m_{33}}qE_z+qE_x+qBv_y,\\
M_3\dot{v}_x+M_4\dot{v}_y&=-\frac{m_{23}}{m_{33}}qE_z+qE_y-qBv_x,\\
\dot{v}_z&=\frac{q}{m_{33}}E_z-\frac{1}{m_{33}}(m_{31}\dot{v}_x+m_{32}\dot{v}_y),
\end{aligned} \tag{2}$$

where the abbreviations

$$\begin{aligned}
M_1&=m_{11}-\frac{m_{13}m_{31}}{m_{33}}, & M_2&=m_{12}-\frac{m_{13}m_{32}}{m_{33}},\\
M_3&=m_{21}-\frac{m_{23}m_{31}}{m_{33}}, & M_4&=m_{22}-\frac{m_{23}m_{32}}{m_{33}},
\end{aligned} \tag{2a}$$

have been made; $m_{jk}$ are the tensor components of $\mathfrak{m}$ in the reference frame chosen. The treatment will be perfectly general until $\mathfrak{m}$ in the cubic reference frame is specified. For $n$-germanium, it has been demonstrated[3] that

$$\mathfrak{m}_{\text{cubic}}=\tfrac{1}{3}m_t\begin{bmatrix}K+2 & s_3(K-1) & s_2(K-1)\\ s_3(K-1) & K+2 & s_1(K-1)\\ s_2(K-1) & s_1(K-1) & K+2\end{bmatrix}, \tag{3}$$

* The research reported in this document was supported jointly by the Army, Navy, and Air Force under contract with the Massachusetts Institute of Technology.
† Present address: Edgerton, Germeshausen, and Grier, Inc., 160 Brookline Avenue, Boston 15, Massachusetts.
[1] L. Gold, Phys. Rev. **104**, 1580 (1956).
[2] N. Sclar and E. Burstein, J. Phys. Chem. Solids **2**, 1 (1957).
[3] L. Gold and L. M. Roth, Phys. Rev. **103**, 61 (1956).

TABLE I. Transformation matrices from cubic to magnetic coordinates. Case (a) for $\mathbf{E}_{100}$, $\mathbf{B}$ in (010) plane with $E_x=0$, $E_y=E\sin\theta$, $E_z=E\cos\theta$. Case (b) for $\mathbf{E}_{110}$, $\mathbf{B}$ in $(1\bar{1}0)$ plane with $E_x=E\cos\theta$, $E_y=0$, $E_z=E\sin\theta$. Case (c) for $\mathbf{E}_{100}$, $\mathbf{B}$ in (100) plane with $\theta$ angle between $\mathbf{B}$ and [010] direction. Case (d) for $\mathbf{E}_{\bar{1}10}$, $\mathbf{B}$ in $(\bar{1}10)$ plane with $\theta$ angle between $\mathbf{B}$ and [001] direction.

| | (a) $x_1'$ | $x_2'$ | $x_3'$ | | (b) $x_1'$ | $x_2'$ | $x_3'$ |
|---|---|---|---|---|---|---|---|
| $x_1$ | 0 | $\sin\theta$ | $\cos\theta$ | $x_1$ | $\frac{1}{2}\sqrt{2}\cos\theta$ | $-\frac{1}{2}\sqrt{2}$ | $\frac{1}{2}\sqrt{2}\sin\theta$ |
| $x_2$ | 1 | 0 | 0 | $x_2$ | $\frac{1}{2}\sqrt{2}\cos\theta$ | $\frac{1}{2}\sqrt{2}$ | $\frac{1}{2}\sqrt{2}\sin\theta$ |
| $x_3$ | 0 | $-\cos\theta$ | $\sin\theta$ | $x_3$ | $-\sin\theta$ | 0 | $\cos\theta$ |
| | (c) $x_1'$ | $x_2'$ | $x_3'$ | | (d) $x_1'$ | $x_2'$ | $x_3'$ |
| $x_1$ | 1 | 0 | 0 | $x_1$ | $-\frac{1}{2}\sqrt{2}$ | $\frac{1}{2}\sqrt{2}\cos\theta$ | $\frac{1}{2}\sqrt{2}\sin\theta$ |
| $x_2$ | 0 | $\sin\theta$ | $\cos\theta$ | $x_2$ | $\frac{1}{2}\sqrt{2}$ | $\frac{1}{2}\sqrt{2}\cos\theta$ | $\frac{1}{2}\sqrt{2}\sin\theta$ |
| $x_3$ | 0 | $-\cos\theta$ | $\sin\theta$ | $x_3$ | 0 | $-\sin\theta$ | $\cos\theta$ |

where $m_t$ is the transverse mass and $K=m_l/m_t$, the ratio of longitudinal to transverse mass. The $s_i$ take on values of $\pm1$ for appropriate designation of each of the four-sets of ellipsoidal energy surfaces. This tensor will need to be transformed later to the magnetic reference frame.

The solution for the system of Eqs. (2) derives from

$$\begin{aligned} N_1d^2v_x/dt^2+N_2dv_x/dt+N_3v_x+N_4=0,\\ N_1d^2v_y/dt^2+N_2dv_y/dt+N_3v_y+N_5=0, \end{aligned} \tag{4}$$

which have the coefficients

$$N_1=M_1M_4-M_2M_3,\quad N_2=(M_3-M_2)qB,\quad N_3=q^2B^2,$$

$$N_4=q^2B\left(\frac{m_{23}}{m_{33}}E_z-E_y\right),\quad N_5=q^2B\left(E_x-\frac{m_{13}}{m_{33}}E_z\right). \tag{4a}$$

The velocity expressions resulting from (4) are of the form

$$v_{x,y}=\text{const}\ e^{-\frac{1}{2}(N_2/N_1)t}\cos\omega t-\frac{N_{4,5}}{N_3}. \tag{5}$$

Physically meaningful solutions must be free of the damping exponential factor—in fact, the mass tensor $\|m_{jk}\|$ must be symmetrical with $m_{jk}=m_{kj}$, as will be demonstrated. Hence $M_2=M_3$ and $N_2=0$. The angular frequency $\omega$ is given by

$$\omega^2=\frac{N_3}{N_1}=\frac{q^2B^2}{M_1M_4-M_2^2}. \tag{6}$$

A secular solution for the cyclotron frequencies with $\mathbf{B}$ arbitrarily oriented has already been reported elsewhere.[4]

The specific character of the trajectories will very much depend upon the relative orientations of $\mathbf{B}$ and $\mathbf{E}$ so that further discussion requires specialization to systems of interest. For these are selected $\mathbf{E}$ along a high-symmetry direction with $\mathbf{B}$ rotated either in the plane to which $\mathbf{E}$ is orthogonal or in the high-symmetry plane containing $\mathbf{E}$.

### A. High-Symmetry "Longitudinal" Alignments

Consideration is given to (1) $\mathbf{E}_{100}$ with $\mathbf{B}$ in (010) plane, and (2) $\mathbf{E}_{110}$ with $\mathbf{B}$ in $(1\bar{1}0)$. For the former the angle $\theta$ is between the directions of $\mathbf{E}$ and $\mathbf{B}$; $\theta$ in the latter case is between $\mathbf{B}$ and the [001] direction. Table I contains the respective transformation matrices from which $\|m_{jk}\|$ is evaluated via

$$m_{j'k'}=\frac{\partial x_{j'}}{\partial x_j}\frac{\partial x_{k'}}{\partial x_k}m_{jk}=\tfrac{1}{3}m_ta_{jk}, \tag{7}$$

where $m_t$ is the transverse mass in the ellipsoid reference frame. The $a_{jk}$ are found in Table II.

The system of Eqs. (2) now may be written in the form

$$\begin{aligned} M_1\dot{v}_x+M_2\dot{v}_y=E_1+qBv_y,\\ M_2\dot{v}_x+M_4\dot{v}_y=E_2-qBv_x, \end{aligned} \tag{8}$$

where (1) $\mathbf{E}_{100}$ and $\mathbf{B}$ in (010) plane has $E_x=0$,

TABLE II. Components of the mass tensor in the magnetic reference frame $m_{j'k'}=\frac{1}{3}m_ta_{jk}$. See reference 1 for mass tensor in cubic reference frame and the meaning of the $s_j$ for the ellipsoidal energy surfaces of germanium. $K=m_l/m_t$.

| | (a) $\mathbf{E}_{100}$, $\mathbf{B}$ in (010) plane | (b) $\mathbf{E}_{110}$, $\mathbf{B}$ in (110) plane |
|---|---|---|
| $a_{11}$ | $K+2$ | $K+2+(K-1)[s_3\cos^2\theta-\sqrt{2}(s_1+s_2)\sin\theta\cos\theta]$ |
| $a_{22}$ | $K+2-2s_2(K-1)\sin\theta\cos\theta$ | $K+2-s_3(K-1)$ |
| $a_{33}$ | $K+2+2s_2(K-1)\sin\theta\cos\theta$ | $K+2+(K-1)[s_3\sin^2\theta+\sqrt{2}(s_1+s_2)\sin\theta\cos\theta]$ |
| $a_{12}$ | $(K-1)(s_3\sin\theta-s_1\cos\theta)$ | $\frac{1}{2}\sqrt{2}(K-1)(s_2-s_1)\sin\theta$ |
| $a_{13}$ | $(K-1)(s_3\cos\theta+s_1\sin\theta)$ | $(K-1)[s_3\sin\theta\cos\theta+\frac{1}{2}\sqrt{2}(s_1+s_2)(\cos^2\theta-\sin^2\theta)]$ |
| $a_{23}$ | $s_2(K-1)(\sin^2\theta-\cos^2\theta)$ | $\frac{1}{2}\sqrt{2}(K-1)(s_1-s_2)\cos\theta$ |
| | (c) $\mathbf{E}_{100}$, $\mathbf{B}$ in (100) plane | (d) $\mathbf{E}_{\bar{1}10}$, $\mathbf{B}$ in $(\bar{1}10)$ plane |
| $a_{11}$ | $K+2$ | $K+2-s_3(K-1)$ |
| $a_{22}$ | $K+2-2s_1(K-1)\sin\theta\cos\theta$ | $K+2+(K-1)[s_3\cos^2\theta-\sqrt{2}(s_1+s_2)\sin\theta\cos\theta]$ |
| $a_{33}$ | $K+2+2s_1(K-1)\sin\theta\cos\theta$ | $K+2+(K-1)[s_3\sin^2\theta+\sqrt{2}(s_1+s_2)\sin\theta\cos\theta]$ |
| $a_{12}$ | $(K-1)(s_3\sin\theta-s_2\cos\theta)$ | $(s_2-s_1)(K-1)\frac{1}{2}\sqrt{2}\sin\theta$ |
| $a_{13}$ | $(K-1)(s_3\cos\theta+s_2\sin\theta)$ | $(s_1-s_2)(K-1)\frac{1}{2}\sqrt{2}\cos\theta$ |
| $a_{23}$ | $s_1(K-1)(\sin^2\theta-\cos^2\theta)$ | $(K-1)[\frac{1}{2}\sqrt{2}(s_1+s_2)(\cos^2\theta-\sin^2\theta)+s_3\sin\theta\cos\theta]$ |

[4] L. Gold, J. Electronics 2, 131 (1956).

$E_y=E\sin\theta$, $E_z=E\cos\theta$, whence

$$E_1=-\frac{m_{13}}{m_{33}}qE\cos\theta, \quad E_2=qE\left(\sin\theta-\frac{m_{23}}{m_{33}}\cos\theta\right); \quad (8a)$$

(2) $\mathbf{E}_{110}$ and $\mathbf{B}$ in $(1\bar{1}0)$ plane has $E_x=E\cos\theta$, $E_y=0$, $E_z=E\sin\theta$, whence

$$E_1=qE\left(\cos\theta-\frac{m_{13}}{m_{33}}\sin\theta\right), \quad E_2=-qE\frac{m_{23}}{m_{33}}\sin\theta. \quad (8b)$$

The complete solution for (8) entails considerable labor. The results

$$\begin{aligned} v_x&=\frac{E_2}{qB}(1-\cos\omega t)+\frac{1}{\omega\mu}(M_4E_1-M_2E_2)\sin\omega t,\\ v_y&=-\frac{E_1}{qB}(1-\cos\omega t)+\frac{1}{\omega\mu}(M_1E_2-M_2E_1)\sin\omega t, \end{aligned} \quad (9)$$

where $\mu=M_1M_4-M_2^2$, can be shown to satisfy (8) for the initial conditions $v_x=v_y=0$ at $t=0$. The associated displacements are

$$\begin{aligned} x&=\frac{E_2}{qB}\left(t-\frac{1}{\omega}\sin\omega t\right)+\frac{1}{q^2B^2}(M_2E_2-M_4E_1)(\cos\omega t-1),\\ y&=-\frac{E_1}{qB}\left(t-\frac{1}{\omega}\sin\omega t\right)+\frac{1}{q^2B^2}(M_2E_1-M_1E_2)(\cos\omega t-1), \end{aligned} \quad (10)$$

which fulfill the initial requirements $x=y=0$ at $t=0$. The $z$ components of velocity and displacement involve Eqs. (9) and (10) in the following way:

$$\begin{aligned} v_z&=\frac{q}{m_{33}}E_zt-\frac{1}{m_{33}}(m_{31}v_x+m_{32}v_y),\\ z&=\frac{1}{2}\frac{q}{m_{33}}E_zt^2-\frac{1}{m_{33}}(m_{31}x+m_{32}y), \end{aligned} \quad (11)$$

with the initial conditions, $v_z=z=0$ at $t=0$, built in.

### B. High-Symmetry Transverse Alignments

A number of approaches may be used to elaborate these solutions. Indeed, the analysis for the longitudinal alignments, with suitable transformations, can be employed for this purpose, preserving the mass-tensor components listed in Table II.

However, a more generalized attack utilizes the Cartesian reference frame defined by $\mathbf{E}\perp\mathbf{B}$, where $\mathbf{B}=\mathbf{k}B_z$ and $\mathbf{E}=\mathbf{i}E_x$. Hence, Eqs. (2) reduce to

$$\begin{aligned} M_1\dot{v}_x+M_2\dot{v}_y&=qE+qBv_y,\\ M_3\dot{v}_x+M_4\dot{v}_y&=-qBv_x, \end{aligned} \quad (12)$$

where the $M_i$ are preserved as in (2a). Then with $N_2=N_4=0$ in Eq. (4), the velocity-component solutions are

$$v_x=A\sin\omega t, \quad v_y=(E/B)(\cos\omega t-1)+C\sin\omega t, \quad (13)$$

for the initial conditions $v_x=v_y=0$ at $t=0$. It then follows that the constants $A$ and $C$ are given by

$$C=-(M_2/M_4)A, \quad (14)$$

where

$$A=qE/m^*\omega, \quad m^*=(M_1M_4-M_2^2)/M_4. \quad (15)$$

Now explicit solutions are sought for the two cases: (1) $\mathbf{E}_{100}$ and $\mathbf{B}$ in the (100) plane, and (2) $\mathbf{E}_{110}$, $\mathbf{B}$ in the $(1\bar{1}0)$ plane. The transformation matrices (c) and (d) in Table I for these respective alignments secures the $a_{jk}$ (c) and (d) in Table II; the similarity to the longitudinal cases will be noted. The angle $\theta$ for (1) is that defined by $\mathbf{B}$ and the [010] direction, whereas for (2) it is the angle determined by $\mathbf{B}$ and the [001] direction.

### ENERGY GAIN RELATIONS FOR CONSERVATIVE MOTION

The expressions for the energy are quite different for the longitudinal and transverse combinations. In the Appendix the manner for calculating the longitudinal energy relations is indicated by showing the details for the scalar mass. The result for the tensor mass is of similar form, but with the particular complication of cross terms involving the velocity components. For simplicity the angular dependence of the energy gain may be studied from the nonperiodic contribution alone. Thus for $\mathbf{E}_{100}$ and $\mathbf{B}$ in the (010) plane,

$$\begin{aligned} W&=\frac{1}{2}\frac{q^2E^2t^2}{m_{33}}\cos^2\theta, \quad 0\le\theta<\tfrac{1}{2}\pi\\ m_{33}&=\tfrac{1}{3}m_t[K+2+2s_2(K-1)\sin\theta\cos\theta], \end{aligned} \quad (16)$$

whence for the doubly degenerate ellipsoids the angle-dependent term becomes

$$F(\theta)=\frac{\cos^2\theta/(K+2)}{1\pm[(K-1)/(K+2)]\sin2\theta}. \quad (17)$$

Figure 1(a) depicts the behavior of (17), showing a strong anisotropy with optimal energy gain for $\theta$ about 41°. The same considerations applied to the case $\mathbf{E}_{110}$ and $\mathbf{B}$ in the $(1\bar{1}0)$ plane, where

$$\begin{aligned} W&=\frac{1}{2}\frac{q^2E^2t^2}{m_{33}}\sin^2\theta, \quad 0<\theta\le\tfrac{1}{2}\pi\\ m_{33}&=\tfrac{1}{3}m_t[(K+2)+(K-1)(s_3\sin^2\theta\\ &\qquad +\sqrt{2}(s_1+s_2)\sin\theta\cos\theta] \end{aligned} \quad (18)$$

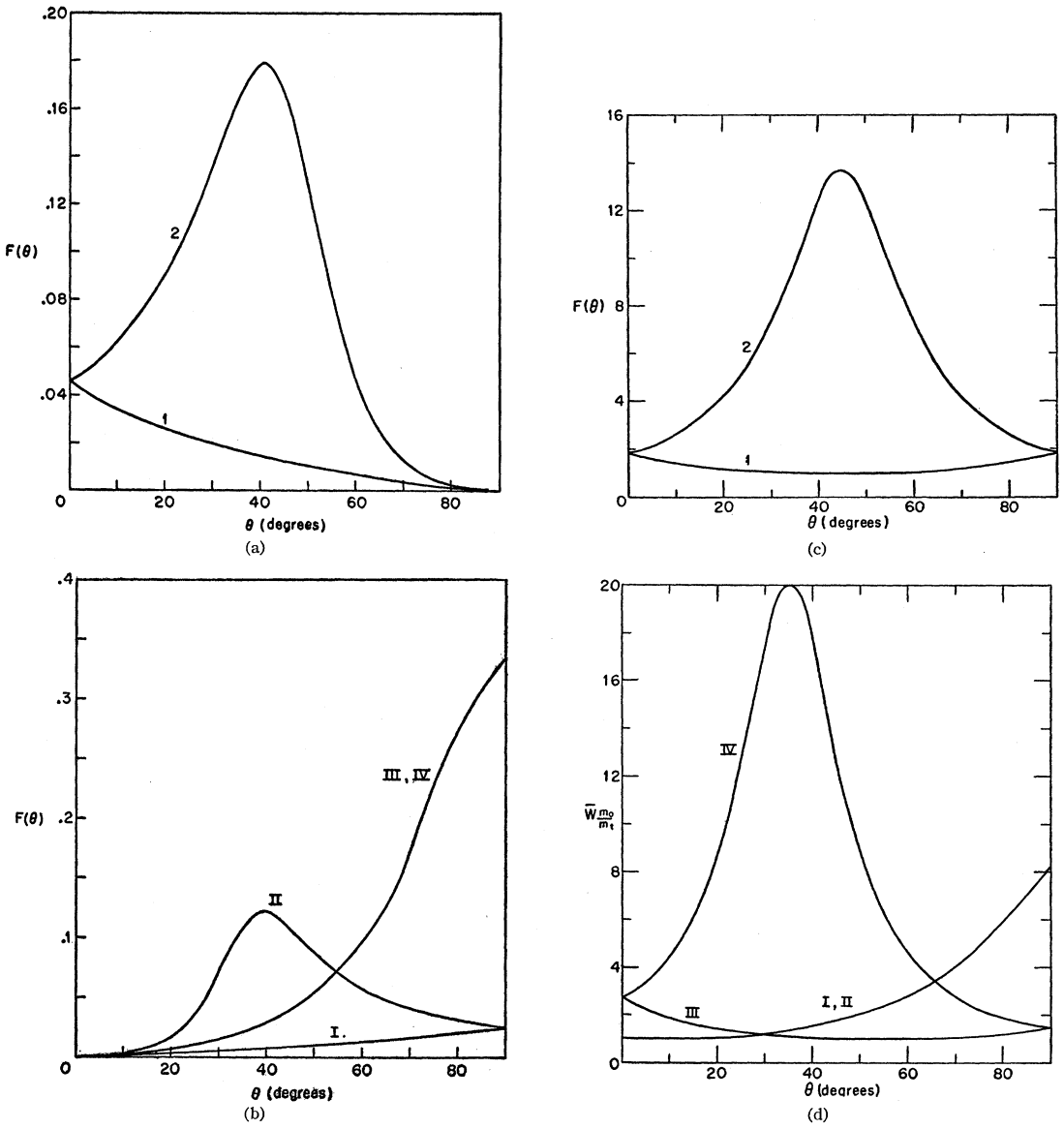


FIG. 1. Angular dependence of the energy gain for electrons in germanium in the absence of scattering with the magnetic field rotated in the following crystallographic planes for the specified directions of the electric field. (a) $\mathbf{E}_{100}$, $\mathbf{B}$ in (010) plane; $\mathbf{E}$ never $\perp$ $\mathbf{B}$. (b) $\mathbf{E}_{110}$, $\mathbf{B}$ in (1$\bar{1}$0) plane; $\mathbf{E}$ never $\perp$ $\mathbf{B}$. (c) $\mathbf{E}_{100}$, $\mathbf{B}$ in (100) plane; $\mathbf{E}$ always $\perp$ $\mathbf{B}$. (d) $\mathbf{E}_{110}$, $\mathbf{B}$ in (110) plane; $\mathbf{E}$ always $\perp$ $\mathbf{B}$. See text for meanings of $F(\theta)$, $\bar{W}(m_0/m_t)$, and numbering of curves.

lead to angular dependence

$$F_{\mathrm{I,II}}(\theta)=\frac{\sin^2\theta/(K+2)}{1+[(K-1)/(K+2)](\sin^2\theta\pm 2\sqrt{2}\,\sin\theta\,\cos\theta)},$$
$$F_{\mathrm{III,IV}}(\theta)=\frac{\sin^2\theta/(K+2)}{1-[(K-1)/(K+2)]\sin^2\theta}. \tag{19}$$

In Fig. 1(b) the energy gain for electrons associated with the four sets of ellipsoids is shown; here, the optimal energy gain is for $\theta=90°$, i.e., for $\mathbf{B}$ along the [110] direction.

Turning next to the transverse energy relations, it is far simpler to deduce the energy gain from the potential energy expression

$$W_{\mathrm{pot}}=qEx=\frac{qEA}{\omega}(1-\cos\omega t). \tag{20}$$

It is convenient to compare energies at the peak of the trajectory, so (20) becomes

$$W_{\mathrm{pot}}=\frac{2q^2E^2}{m^*\omega^2}=2\frac{E^2}{B^2}M_4. \tag{21}$$

Making use of Table II (c) and (d) the specific energy gains are calculated.

Thus for $\mathbf{E}_{100}$ with $\mathbf{B}$ in the orthogonal (010) plane, one obtains

$$W=2\frac{E^2}{B^2}m_t\frac{(2K+1)/(K+2)}{1\pm[(K-1)/(K+2)]\sin 2\theta}. \tag{22}$$

The angle-dependent term is plotted in Fig. 1(c), showing maximal energy gain for $\mathbf{B}_{110}$.

The other orthogonal arrangement of $\mathbf{E}_{110}$ and $\mathbf{B}$ in the (110) plane provides the energy gain relations

$$\begin{aligned} W_{\mathrm{I,II}}&=2m_t\frac{E^2}{B^2}\left(1-\frac{K-1}{K+2}\sin^2\theta\right)^{-1}, \\ W_{\mathrm{III,IV}}&=6m_t\frac{E^2}{B^2}\frac{K/(K+2)}{1+[(K-1)/(K+2)](\sin^2\theta\pm\sqrt{2}\sin 2\theta)}. \end{aligned} \tag{23}$$

These are plotted in a normalized form:

$$\begin{aligned} \bar{W}_{\mathrm{I,II}}&=\frac{m_t}{m_0}F_1(\theta), \\ \bar{W}_{\mathrm{III,IV}}&=3\frac{m_t}{m_0}F_2(\theta), \quad \bar{W}=\frac{W}{2m_0E^2/B^2}, \end{aligned} \tag{23a}$$

in Fig. 1(d) which reveals largest energy gain for the $\mathbf{B}_{112}$ position.

Thus the preliminary analysis based upon the no-scattering limit forcefully demonstrates the enhanced anisotropy to be expected for breakdown in a superposed magnetic field. It will now be appropriate to enter into the more realistic circumstance of scattering contribution to the electron energy gain. Here a detailed comparison of energy gain with and without a magnetic field will be presented.

## NONCONSERVATIVE EQUATIONS OF MOTION FOR ELECTRONS IN GERMANIUM

The formalism already developed for the galvanomagnetic behavior[5] may be taken over with the inclusion of an anisotropic scattering tensor utilized for the zero magnetic field problem dealt with earlier[1]:

$$\nu_{\text{ellipsoidal}}=\begin{bmatrix}\nu_l & 0 & 0\\ 0 & \nu_t & 0\\ 0 & 0 & \nu_t\end{bmatrix} \tag{24}$$

in the equation of motion

$$\frac{d}{dt}(\mathfrak{m}\cdot\mathbf{v})=q\mathbf{E}+q\mathbf{v}\times\mathbf{B}-\nu\cdot(\mathbf{m}\cdot\mathbf{v}). \tag{25}$$

The steady state or terminal velocity solution now becomes (see reference 1)

$$\mathbf{v}=\frac{\boldsymbol{\sigma}\cdot\mathbf{E}}{nq}=\frac{q}{\bar{m}^*\nu_t}\frac{1}{\Delta}\|\sigma_{jk}\|\mathbf{E}. \tag{26}$$

[5] L. Gold and L. M. Roth, Phys. Rev. **107**, 258 (1957).

The modified $\Delta$ and $\sigma_{jk}$ (components of the conductivity tensor $\boldsymbol{\sigma}$) become, because of the anisotropic scattering,

$$\begin{aligned} &\Delta=\det'/KK', \\ &\det'=KK'+b^2+\tfrac{1}{3}(KK'-1)(s_1b_1+s_2b_2+s_3b_3)^2, \\ &\sigma_{11}=1+\frac{3}{2KK'+1}b_1^2, \\ &\sigma_{12}=\frac{3}{2KK'+1}b_1b_2+\frac{KK'+2}{2KK'+1}b_3 \\ &\qquad\qquad+\frac{KK'-1}{2KK'+1}(s_1b_2+s_2b_1-s_3), \\ &\sigma_{13}=\frac{3}{2KK'+1}b_1b_3-\frac{KK'+2}{2KK'+1}b_2 \\ &\qquad\qquad-\frac{KK'-1}{2KK'+1}(s_1b_3+s_3b_1+s_2), \\ &\sigma_{21}=\frac{3}{2KK'+1}b_1b_2-\frac{KK'+2}{2KK'+1}b_3 \\ &\qquad\qquad-\frac{KK'-1}{2KK'+1}(s_1b_2+s_2b_1+s_3), \\ &\sigma_{22}=1+\frac{3}{2KK'+1}b_2^2, \\ &\sigma_{23}=\frac{3}{2KK'+1}b_2b_3+\frac{KK'+2}{2KK'+1}b_1 \\ &\qquad\qquad+\frac{KK'-1}{2KK'+1}(s_2b_3+s_3b_2-s_1), \\ &\sigma_{31}=\frac{3}{2KK'+1}b_1b_3+\frac{KK'+2}{2KK'+1}b_2 \\ &\qquad\qquad+\frac{KK'-1}{2KK'+1}(s_1b_3+s_3b_1-s_2), \\ &\sigma_{32}=\frac{3}{2KK'+1}b_2b_3-\frac{KK'+2}{2KK'+1}b_1 \\ &\qquad\qquad-\frac{KK'-1}{2KK'+1}(s_2b_3+s_3b_2+s_1), \\ &\sigma_{33}=1+\frac{3}{2KK'+1}b_3^2, \end{aligned} \tag{27, 28}$$

where

$$\mathbf{b}=q\mathbf{B}/m_t\nu_t, \quad K'=\nu_l/\nu_t, \tag{29}$$

TABLE III. Relative energy gain for three values of the ratio of Larmor to scattering frequency $b=\infty$, 1, and 0.1; the influence of the scattering anisotropy is illustrated by passage from $K'=1$ to $\infty$.

| | | I | | II | | III | | IV | |
|---|---|---|---|---|---|---|---|---|---|
| | $hkl$ in $B_{hkl}$ | $K'=1$ | $K'\to\infty$ | $K'=1$ | $K'\to\infty$ | $K'=1$ | $K'\to\infty$ | $K'=1$ | $K'\to\infty$ |
| | | | | $b\to\infty$ | | | | | |
| $E_{100}$ and $E_{\bar{1}00}$ | $B_{100}$ | 0.87610 | 0 | 0.87610 | 0 | 0.87610 | 0 | 0.87610 | 0 |
| | $B_{110}$ | 0.23505 | 0 | 3.2124 | 3.375 | 0.23505 | 0 | 3.2124 | 3.375 |
| | $B_{010}$ | 0 | 0 | 0 | 0 | 0 | 0 | 0 | 0 |
| | $B_{\bar{1}10}$ | 3.2124 | 3.375 | 0.23505 | 0 | 3.2124 | 3.375 | 0.23505 | 0 |
| | $B_{\bar{1}00}$ | 0.87610 | 0 | 0.87610 | 0 | 0.87610 | 0 | 0.87610 | 0 |
| | $B_{001}$ | 0 | 0 | 0 | 0 | 0 | 0 | 0 | 0 |
| | $B_{011}$ | 0 | 0 | 0 | 0 | 0 | 0 | 0 | 0 |
| | $B_{111}$ | 0.10708 | 0 | 0.68837 | 0 | 0.68837 | 0 | 0.68837 | 0 |
| $E_{\bar{1}10}$ | $B_{110}$ | 0 | 0 | 0 | 0 | 0 | 0 | 0 | 0 |
| | $B_{111}$ | 0 | 0 | 0 | 0 | 0 | 0 | 0 | 0 |
| | $B_{112}$ | 0 | 0 | 0 | 0 | 0 | 0 | 0 | 0 |
| | $B_{001}$ | 0 | 0 | 0 | 0 | 0 | 0 | 0 | 0 |
| | $B_{100}$ and $B_{010}$ | 0.43805 | 0 | 0.43805 | 0 | 0.43805 | 0 | 0.43805 | 0 |
| | $B_{\bar{1}10}$ | 6.4247 | 6.75 | 0.47010 | 0 | 6.4247 | 6.75 | 0.47010 | 0 |
| | $B_{\bar{1}00}$ | 0.43805 | 0 | 0.43805 | 0 | 0.43805 | 0 | 0.43805 | 0 |
| | $B_{121}$ | 0.029929 | 0 | 0.10252 | 0 | 0.10252 | 0 | 0.53540 | 0.5625 |
| | $B_{120}$ | 0.05181 | 0 | 0.28344 | 0 | 0.05181 | 0 | 0.28344 | 0 |
| | $B_{\bar{1}11}$ | 1.3767 | 0 | 0.21416 | 0 | 1.3767 | 0 | 1.3767 | 0 |
| | $B_{\bar{1}12}$ | 0.4101 | 0 | 0.1197 | 0 | 0.4101 | 0 | 2.1416 | 2.25 |
| $E_{111}$ | $B_{100}$ | 0.29203 | 0 | 0.29203 | 0 | 0.29203 | 0 | 0.29203 | 0 |
| | $B_{111}$ | 0.32124 | 0 | 2.0651 | 0 | 2.0651 | 0 | 2.0651 | 0 |
| | | | | $b=1$ | | | | | |
| $E_{100}$ and $E_{\bar{1}00}$ | $B_{100}$ | 3.4474 | 3.375 | 3.4474 | 3.375 | 3.4474 | 3.375 | 3.4474 | 3.375 |
| | $B_{110}$ | 2.7035 | 2.7 | 4.3342 | 4.5 | 2.7035 | 2.7 | 4.3342 | 4.5 |
| | $B_{010}$ | 3.2124 | 3.375 | 3.2124 | 3.375 | 3.2124 | 3.375 | 3.2124 | 3.375 |
| | $B_{\bar{1}10}$ | 4.3342 | 4.5 | 2.7035 | 2.7 | 4.3342 | 4.5 | 2.7035 | 2.7 |
| | $B_{\bar{1}00}$ | 3.4474 | 3.375 | 3.4474 | 3.375 | 3.4474 | 3.375 | 3.4474 | 3.375 |
| | $B_{001}$ | 3.2124 | 3.375 | 3.2124 | 3.375 | 3.2124 | 3.375 | 3.2124 | 3.375 |
| | $B_{011}$ | 2.6081 | 2.7 | 2.6081 | 2.7 | 4.0274 | 4.5 | 4.0274 | 4.5 |
| | $B_{111}$ | 2.2487 | 2.5 | 3.8919 | 4.05 | 3.8919 | 4.05 | 3.8919 | 4.05 |
| $E_{\bar{1}10}$ | $B_{110}$ | 3.8167 | 4.05 | 2.2436 | 2.5 | 3.8167 | 4.05 | 2.2436 | 2.5 |
| | $B_{111}$ | 3.2124 | 3.375 | 2.0386 | 2.025 | 5.5600 | 6.075 | 2.0386 | 2.025 |
| | $B_{112}$ | 3.3644 | 3.5735 | 1.8680 | 1.8409 | 6.1188 | 6.75 | 1.8680 | 1.8409 |
| | $B_{001}$ | 4.7010 | 5.0625 | 1.7237 | 1.6875 | 4.7010 | 5.0625 | 1.7237 | 1.6875 |
| | $B_{100}$ and $B_{010}$ | 4.8186 | 5.0625 | 1.8412 | 1.6875 | 4.8186 | 5.0625 | 1.8412 | 1.6875 |
| | $B_{\bar{1}10}$ | 6.4247 | 6.75 | 1.5903 | 1.35 | 6.4247 | 6.75 | 1.5903 | 1.35 |
| | $B_{\bar{1}00}$ | 4.8186 | 5.0625 | 1.8412 | 1.6875 | 4.8186 | 5.0625 | 1.8412 | 1.6875 |
| | $B_{121}$ | 3.4055 | 3.5735 | 1.8892 | 1.8409 | 5.1157 | 5.5227 | 2.2691 | 2.25 |
| | $B_{120}$ | 3.9857 | 4.2188 | 2.1448 | 2.1094 | 3.9857 | 4.2188 | 2.1448 | 2.1094 |
| | $B_{\bar{1}11}$ | 5.7452 | 6.075 | 1.2849 | 1.125 | 5.7452 | 6.075 | 2.2240 | 2.025 |
| | $B_{\bar{1}12}$ | 5.1794 | 5.5227 | 1.3000 | 1.1912 | 5.1794 | 5.5227 | 2.3455 | 2.25 |
| $E_{111}$ | $B_{100}$ | 0.31340 | 0 | 4.2832 | 4.5 | 4.2832 | 4.5 | 4.2832 | 4.5 |
| | $B_{111}$ | 0.32124 | 0 | 5.6855 | 5.4 | 5.6855 | 5.4 | 5.6855 | 5.4 |
| | | | | $b=0.1$ | | | | | |
| $E_{100}$ | $B_{100}$ | 4.3774 | 4.485 | 4.3774 | 4.485 | 4.3774 | 4.485 | 4.3774 | 4.485 |
| | $B_{110}$ | 4.3620 | 4.4702 | 4.3897 | 4.5 | 4.3620 | 4.4702 | 4.3897 | 4.5 |
| | $B_{010}$ | 4.3742 | 4.485 | 4.3742 | 4.485 | 4.3742 | 4.485 | 4.3742 | 4.485 |
| | $B_{\bar{1}10}$ | 4.3897 | 4.5 | 4.3620 | 4.4702 | 4.3897 | 4.5 | 4.3620 | 4.4702 |
| | $B_{\bar{1}00}$ | 4.3774 | 4.485 | 4.3774 | 4.485 | 4.3774 | 4.485 | 4.3774 | 4.485 |
| | $B_{001}$ | 4.3742 | 4.485 | 4.3742 | 4.485 | 4.3742 | 4.485 | 4.3742 | 4.485 |
| | $B_{011}$ | 4.3604 | 4.4702 | 4.3604 | 4.4702 | 4.3880 | 4.5 | 4.3880 | 4.5 |
| | $B_{111}$ | 4.4421 | 4.4554 | 4.3845 | 4.4950 | 4.3845 | 4.4950 | 4.3845 | 4.4950 |
| $E_{\bar{1}10}$ | $B_{110}$ | 6.3811 | 6.7053 | 2.3546 | 2.25 | 6.3811 | 6.7053 | 2.3546 | 2.25 |
| | $B_{111}$ | 6.3631 | 6.6832 | 2.3517 | 2.2475 | 6.4148 | 6.7425 | 2.3521 | 2.2475 |
| | $B_{112}$ | | 6.6905 | | 2.2450 | | 6.75 | | 2.2450 |
| | $B_{001}$ | 6.4013 | 6.7276 | 2.3471 | 2.2425 | 6.4013 | 6.7276 | 2.3471 | 2.2425 |
| | $B_{010}$ | 6.4029 | 6.7276 | 2.3487 | 2.2425 | 6.4029 | 6.7276 | 2.3487 | 2.2425 |
| | $B_{\bar{1}10}$ | 6.4247 | 6.75 | 2.3429 | 2.2351 | 6.4247 | 6.75 | 2.3429 | 2.2351 |
| | $B_{\bar{1}00}$ | 6.4029 | 6.7276 | 2.3487 | 2.2425 | 6.4029 | 6.7276 | 2.3487 | 2.2425 |
| | $B_{121}$ | 6.3681 | 6.6905 | 2.3499 | 2.2450 | 6.4083 | 6.7350 | 2.3548 | 2.25 |
| | $B_{120}$ | | | | | | | | |
| | $B_{\bar{1}11}$ | 6.4169 | 6.7425 | 2.3345 | 2.2277 | 6.4169 | 6.7425 | 2.3542 | 2.2475 |
| | $B_{\bar{1}12}$ | 6.4101 | 6.7350 | 2.3370 | 2.2302 | 6.4101 | 6.7350 | 2.3567 | 2.25 |
| $E_{111}$ | $B_{100}$ | 0.32113 | 0 | 5.7267 | 5.9801 | 5.7267 | 5.9801 | 5.7267 | 5.9801 |
| | $B_{111}$ | 0.32124 | 0 | 5.7409 | 5.9933 | 5.7409 | 5.9933 | 5.7409 | 5.9933 |

TABLE III.—*Continued.*

| | *hkl* in $B_{hkl}$ | I $K'=1$ | I $K'\to\infty$ | II $K'=1$ | II $K'\to\infty$ | III $K'=1$ | III $K'\to\infty$ | IV $K'=1$ | IV $K'\to\infty$ |
|---|---|---|---|---|---|---|---|---|---|
| | | | | $b\to\infty$ | | | | | |
| $E_{\bar{1}11}$ | $B_{\bar{1}10}$ | 4.2832 | 4.5 | 0.31340 | 0 | 4.2832 | 4.5 | 0.31340 | 0 |
| $E_{\bar{1}12}$ | | 2.1416 | 2.25 | 0.15670 | 0 | 2.1416 | 2.25 | 0.15670 | 0 |
| $E_{001}$ | | 0 | 0 | 0 | 0 | 0 | 0 | 0 | 0 |
| | | | | $b=1$ | | | | | |
| $E_{\bar{1}11}$ | $B_{\bar{1}10}$ | 5.6769 | 6.0 | 0.31806 | 0 | 5.6769 | 6.0 | 3.5410 | 3.6 |
| $E_{\bar{1}12}$ | | 4.9290 | 5.15 | 0.65732 | 0.45 | 4.9290 | 5.25 | 3.8803 | 4.05 |
| $E_{001}$ | | 4.1812 | 4.5 | 2.6081 | 2.7 | 4.1812 | 4.5 | 2.6081 | 2.7 |
| | | | | $b=0.1$ | | | | | |
| $E_{\bar{1}11}$ | $B_{\bar{1}10}$ | 5.7458 | 6.0 | 0.32118 | 0 | 5.7458 | 6.0 | 5.7097 | 5.9603 |
| $E_{\bar{1}12}$ | | 5.0669 | 5.25 | 0.99369 | 0.745 | 5.0669 | 5.25 | 6.48 | 6.75 |
| $E_{001}$ | | 4.3880 | 4.5 | 4.3604 | 4.4702 | 4.3880 | 4.5 | 4.3604 | 4.4702 |

and the $b_i$ are the components of **b**. The $s_i$ values are given in the related papers.[3,5] For the velocity components themselves it follows that

$$v_i=\frac{qE}{\bar{m}^*\nu_t}\frac{1}{\Delta}(l_1\sigma_{1i}+l_2\sigma_{2i}+l_3\sigma_{3i}),\quad i=1,2,3. \tag{30}$$

The $l_i$ are the direction cosines for the electric vector **E**.

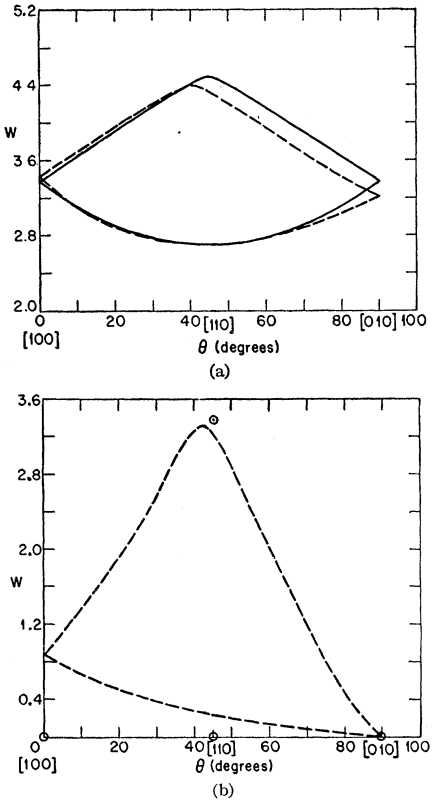


FIG. 2. Effect of scattering on angular dependence of electron energy gain for longitudinal alignment $\mathbf{E}_{100}$, **B** in (010) plane; compare with Fig. 1(a). (a) Cyclotron and scattering frequencies comparable, $b=1$. Isotropic scattering $K'=1$ for dashed curve, whereas extreme anisotropy $K'\to\infty$ for solid curve. (b) Cyclotron frequency far greater than scattering frequency, $b\to\infty$. Dashed curve, $K'=1$; and ⊙, points for $K'\to\infty$.

## ENERGY GAIN IN THE PRESENCE OF SCATTERING

The kinetic energy relation is given by[1]

$$W=\frac{1}{2}\sum_{i=1}^{3} m_{ij}v_iv_j,\quad j=1,2,3$$

$$=\tfrac{1}{2}\{m_{11}v_x^2+m_{22}v_y^2+m_{33}v_z^2+2m_{12}v_xv_y+2m_{13}v_xv_z+2m_{23}v_yv_z\}, \tag{31}$$

where the $m_{ij}$ are the mass tensor components contained in Eq. (3).

Thus the directional energy for electrons associated with the four sets of ellipsoidal energy surfaces is calculated from

$$W=\frac{1}{2}\frac{m_t}{3}\frac{q^2E^2}{\bar{m}^{*2}\nu_t^2}\frac{1}{\Delta^2}\{(K+2)\sum_i(l_1\sigma_{1i}+l_2\sigma_{2i}+l_3\sigma_{3i})^2+2(K-1)[s_3(l_1\sigma_{11}+l_2\sigma_{21}+l_3\sigma_{31})\times(l_1\sigma_{12}+l_2\sigma_{22}+l_3\sigma_{32})+\text{c.p.}]\}, \tag{32}$$

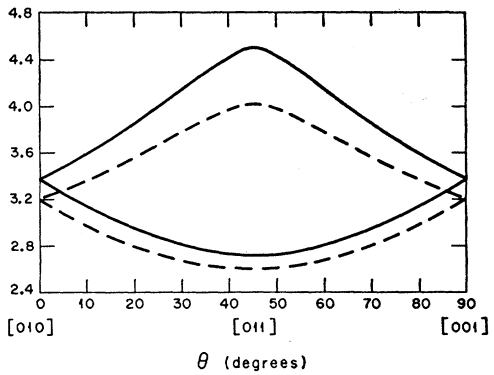


FIG. 3. Effect of scattering on angular dependence of electron energy gain for transverse alignment $\mathbf{E}_{100}$, **B** in (100) plane; compare with Fig. 1(c). Plot shown for $b=1$, dashed curve $K'=1$, solid curve $K'\to\infty$. For $b=0.1$, the angular dependence is more isotropic. The limit $b\to\infty$ corresponds always to $W=0$.

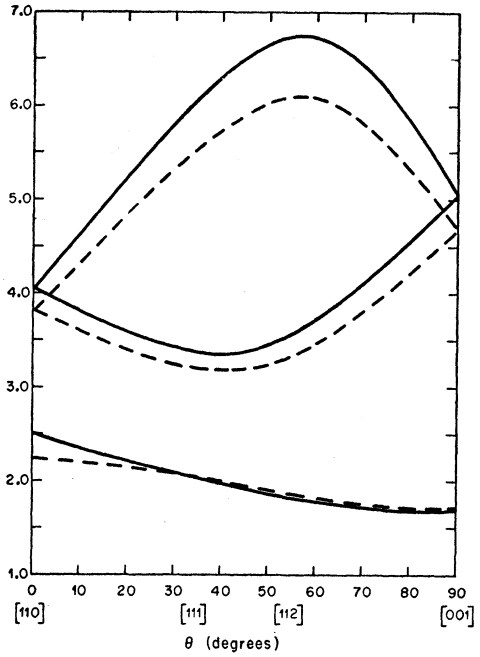


FIG. 4. Effect of scattering on angular dependence of energy gain for transverse alignment $\mathbf{E}_{110}$, $\mathbf{B}$ in (110) plane; compare with Fig. 1(d). Plot shown for $b=1$. The case $b=0.1$ is weakly angle-dependent and for $b\rightarrow\infty$, $W$ always vanishes.

where "c.p." means cyclic permutation. Detailed numerical work based upon Eq. (32) has been performed for $K'=1$ and $K'\rightarrow\infty$ with three common values for $b$, viz., $b=0.1$, 1, and $\infty$. The data are contained in Table III.

Plots displayed in Figs. 2–5 correspond to those of Fig. 1 for the no-scattering limit; the effect of anisotropic scattering may be discerned by comparison of similarly oriented $\mathbf{E}$ and $\mathbf{B}$. Thus (2a) and (2b) reflect the effect of collisions on the behavior exhibited in Fig. 1(a). Figure 3 is to be compared with Fig. 1(c), Fig. 4 with Fig. 1(d), and Figs. 5(a), (b) with Fig. 1(b).

The next set of figures was composed to investigate the influence of a prescribed orientation of magnetic field on the energy gain as the electric vector is rotated. Figure 6 resembles Fig. 1(b) of the $\mathbf{B}=0$ study.[1] Increased anisotropy of scattering does not strongly influence energy gain. This transverse combination of $E$ and $B$ is to be compared with the longitudinal arrangement displayed in Fig. 7, where the peak energy gain shifts from $E_{110}$ to $E_{100}$. The behavior shown in Fig. 1(a) for[1] $B=0$ is to be compared with that contained in Fig. 8; maximum at [112] continues to shift toward [111] until for $b\rightarrow\infty$ this limiting position attained for $K'=1$. The longitudinal alignment corresponding to Fig. 1(a) ($B=0$) exhibits the behavior of Fig. 9; the maximum energy gain now alters from [112] to [110].

Several other interesting combinations of oriented electric and magnetic field have been investigated. Thus, the complementary longitudinal alignment for

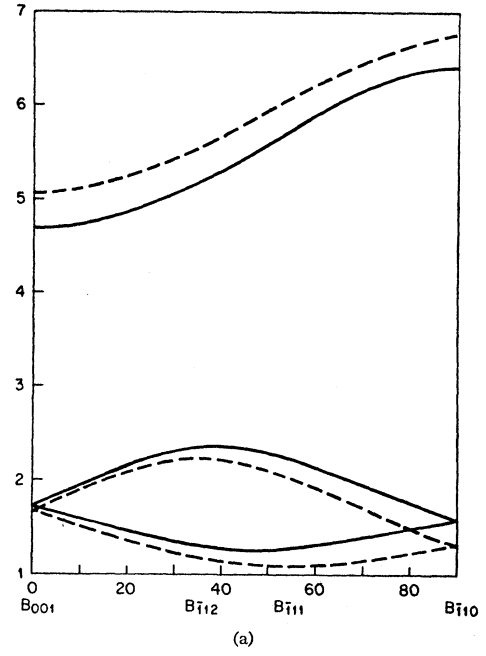


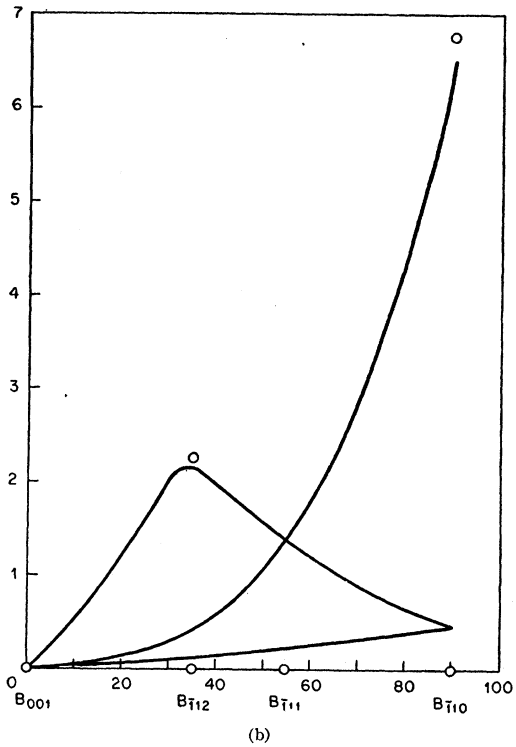


FIG. 5. Effect of scattering on angular dependence of energy gain for longitudinal alignment $\mathbf{E}_{110}$, $\mathbf{B}$ in $(1\bar{1}0)$ plane; compare with Fig. 1(b). The case $b=1$ is depicted in 5(a) with solid curve for $K'=1$ and dashed curve for $K'\rightarrow\infty$; 5(b) shows the effect of $b\rightarrow\infty$ with curve for $K'=1$ and circles for $K'\rightarrow\infty$.

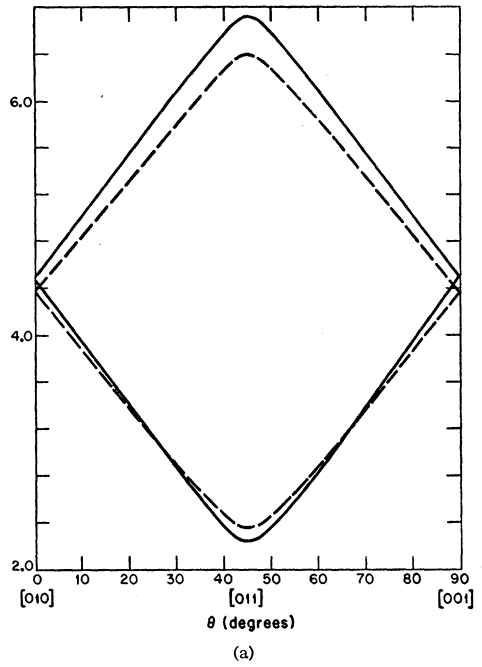


(a)

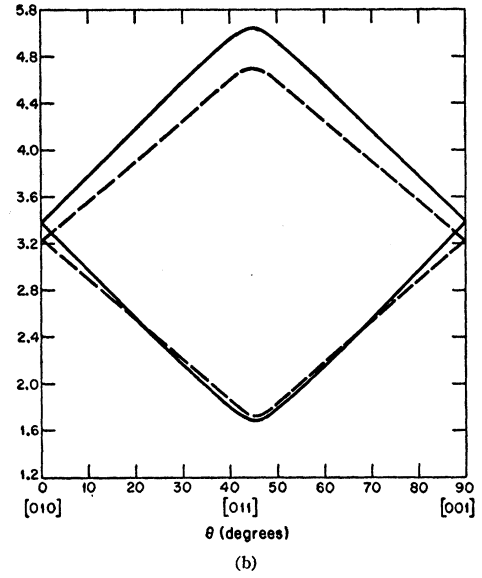


(b)

FIG. 6. Effect of magnetic field on energy gain for **E** rotated in a (100) plane. $\mathbf{B}_{100}$ is in transverse alignment with **E**. Compare with Fig. 1(b) for $B=0.^1$ (a) Scattering effect for $b=0.1$. (b) Scattering effect for $b=1$. In the usual manner for transverse alignment, $b \rightarrow \infty$ produces zero energy gain.

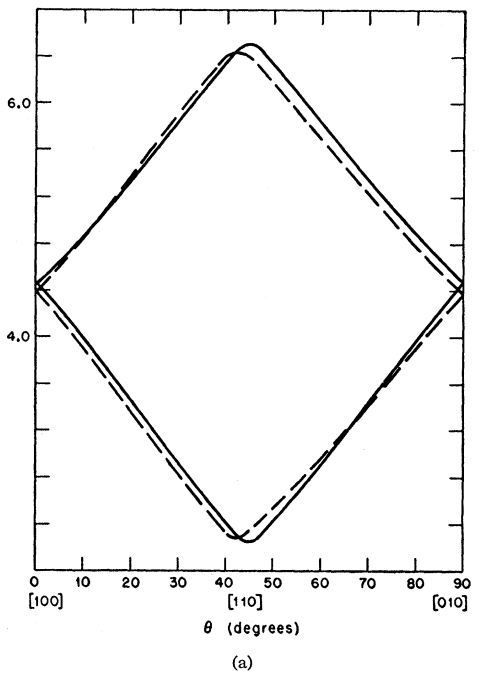


(a)

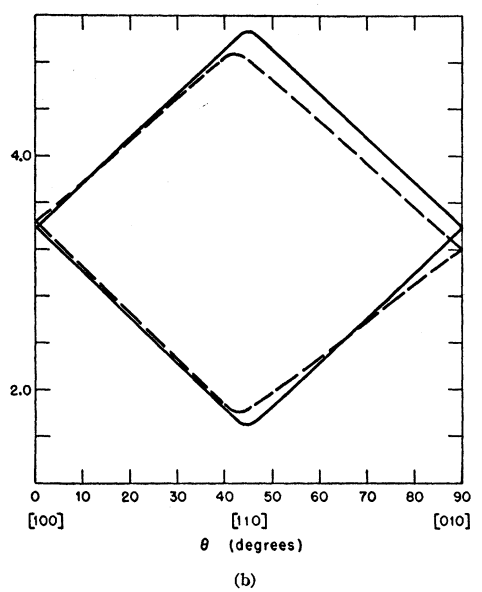


(b)

FIG. 7. Effect of magnetic field on energy gain for **E** rotated in (100) plane, but now $\mathbf{B}_{010}$ is usually longitudinal to **E**. Also compare with Fig. 1(b) for $B=0.^1$ (a) Scattering effect for $b=0.1$. Note the shift in the peak toward [100] for isotropic scattering $K'=1$. (b) Scattering effect for $b=1$; the peak shifts more strongly toward [100] for $K'=1$. The limit $b \rightarrow \infty$ shifts the peak completely to the [100] direction for $K'=1$, but $K' \rightarrow \infty$ gives only zero energy gain.

Fig. 5 is depicted in Fig. 10. Here only two curves are obtained, instead of the three for the four sets of ellipsoidal energy surfaces, and the symmetry is unlike Fig. 1(b) ($B \neq 0$). Finally the parallel situation for Fig. 9 appears in Fig. 11; again only two of the four energy surfaces, instead of three, manifest themselves independently.

## ACKNOWLEDGMENT

It is a pleasure to express appreciation for the M.I.T. Lincoln Laboratory support, particularly with regard to Miss M. Clare Glennon of the Computer Group, who skillfully carried out the many calculations.

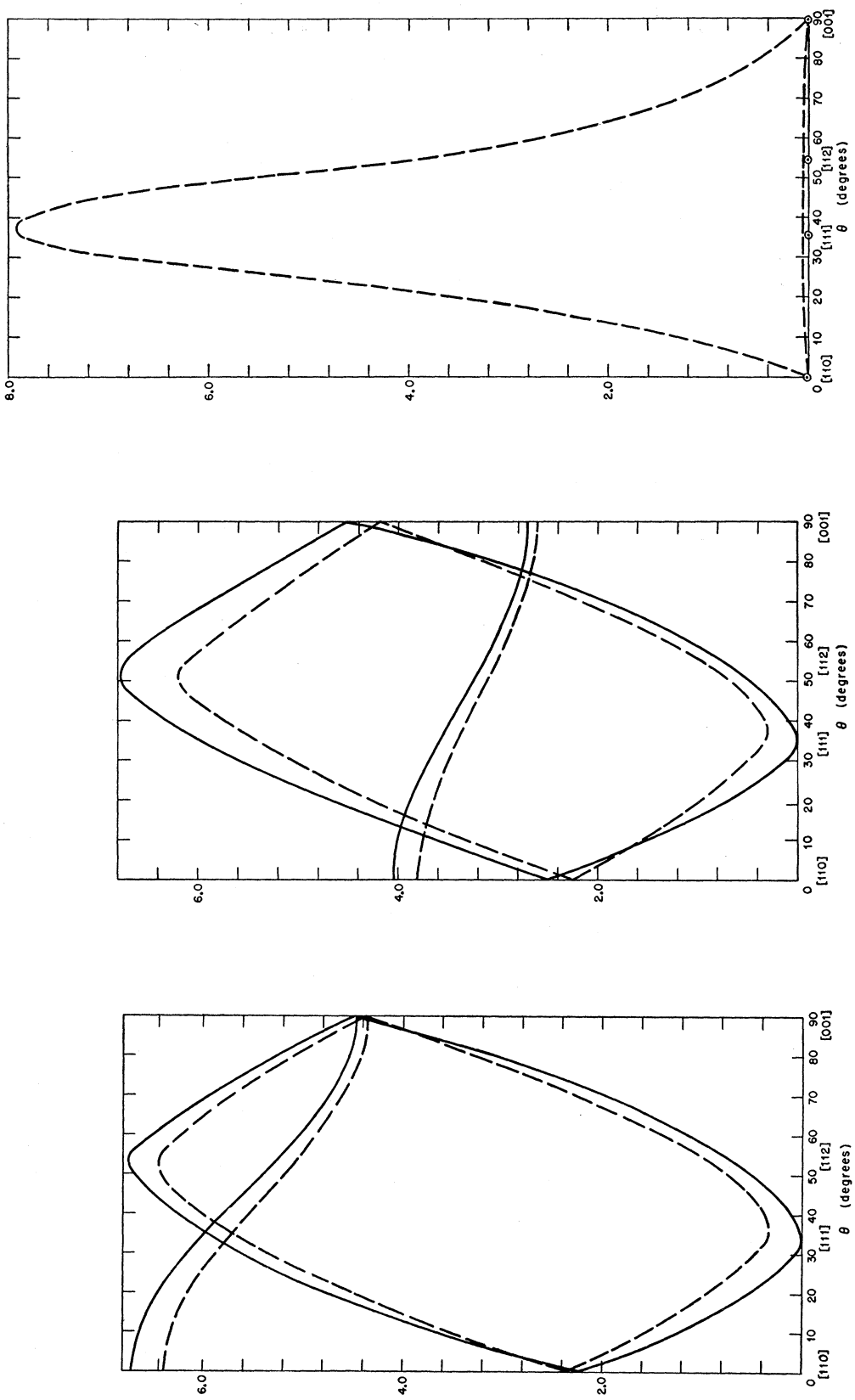


FIG. 8. Effect of magnetic field on energy gain for **E** rotated in (110) plane with $B_{110}$ always transverse to **E**. Compare with Fig. 1(a) for $B=0$.[1] (a) Scattering effect for $b=0.1$. The peak shifts toward [111]. (b) Scattering effect for $b=1$. The peak is still shifting toward [111]. (c) Scattering effect for $b\to\infty$. The peak is now at [111]; $K'\to\infty$ gives zero energy gain.

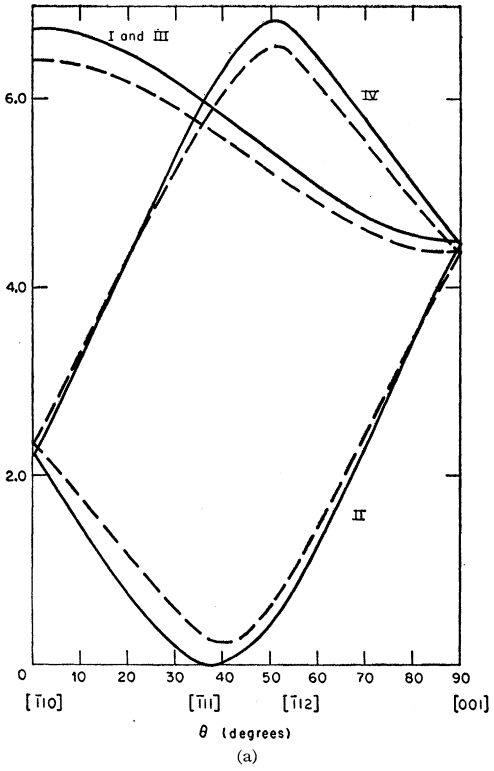

(a)

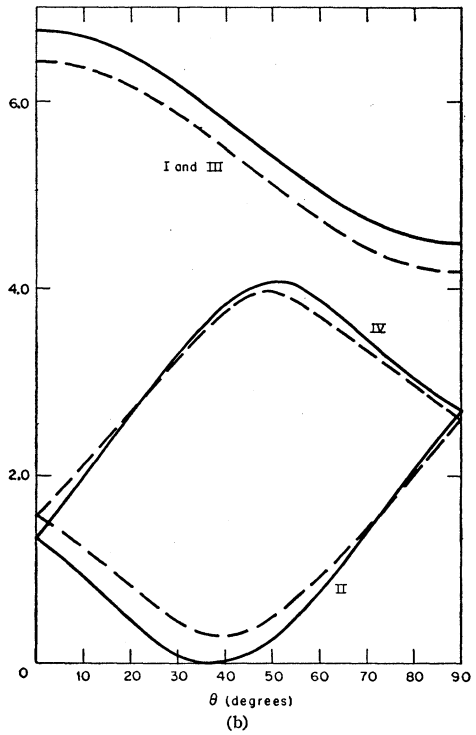

(b)

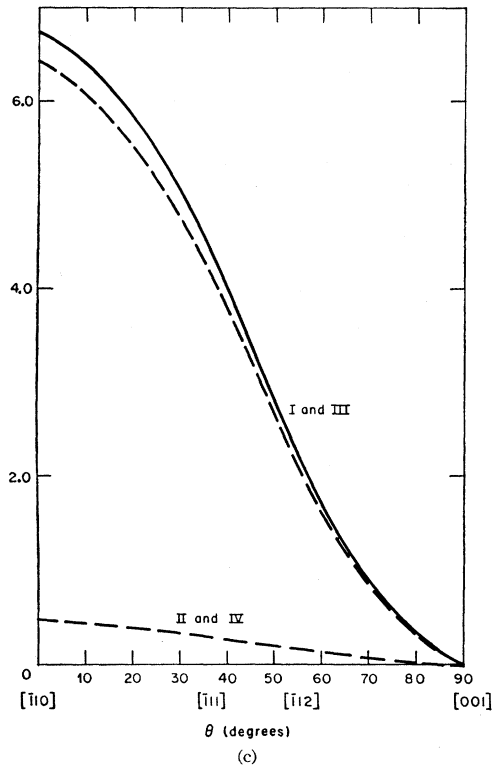

(c)

FIG. 9. Effect of magnetic field on energy gain for **E** rotated in (110) plane but $\mathbf{B}_{\bar{1}10}$ always longitudinal to **E**. Also compare with Fig. 1(a) for $B=0.1$ (a) For $b=0.1$, the peak is still near $[\bar{1}12]$. (b) For $b=1$, the peak is now at $[\bar{1}10]$. (c) For $b=\infty$, the peak is still $[\bar{1}10]$, but the anisotropy is very strong.

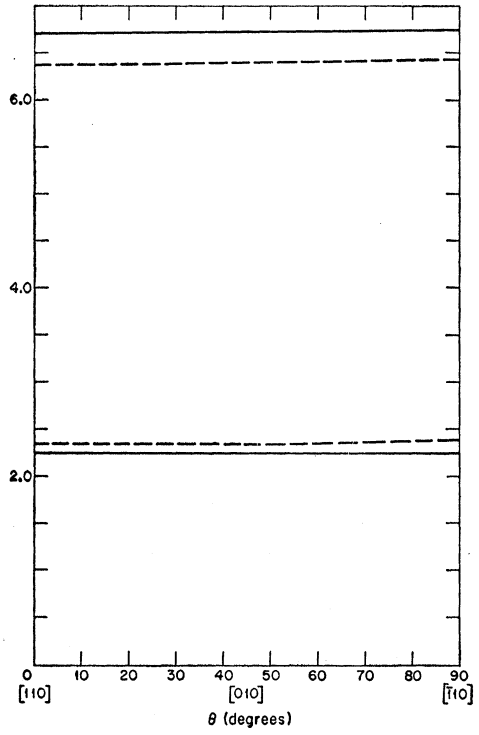


(a)

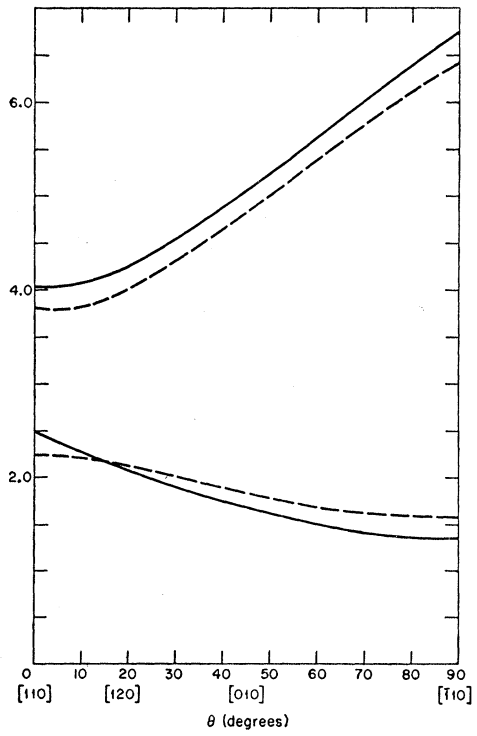


(b)

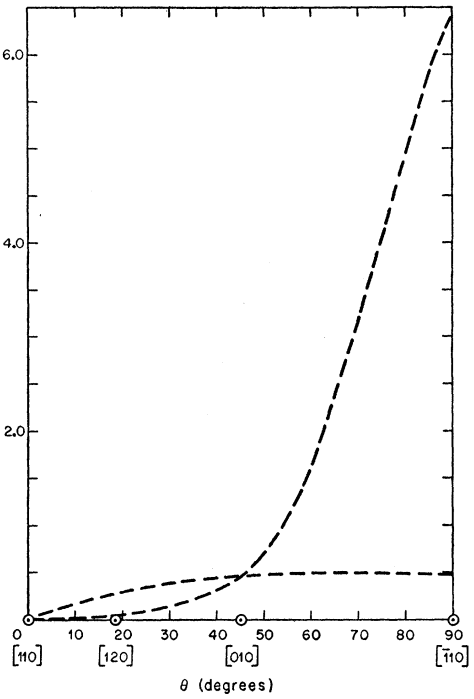


(c)

FIG. 10. Energy gain for $\mathbf{E}_{\bar{1}10}$, $\mathbf{B}$ rotated in (110) plane in constant longitudinal alignment. Compare with Fig. 5. (a) $b=0.1$; – – – $K'=1$, solid $K' \to \infty$. (b) $b=1.0$; – – – $K'=1$, solid $K' \to \infty$. (c) $b \to \infty$; ⊙ circles for $K' \to \infty$.

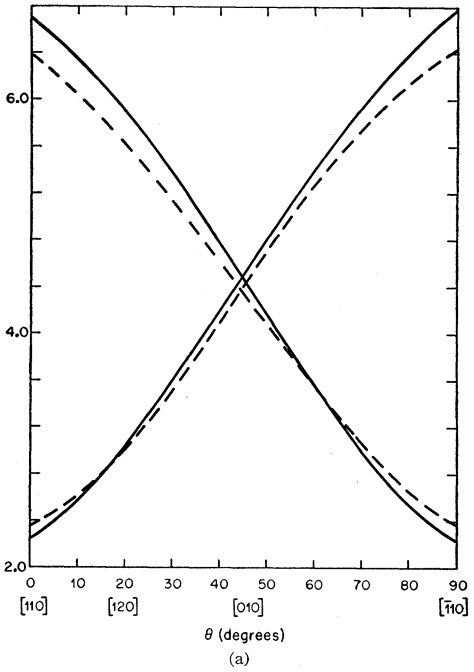


(a)

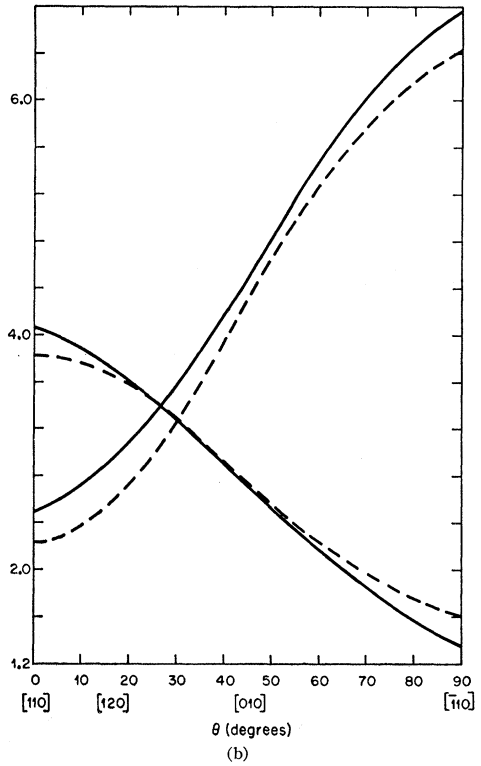


(b)

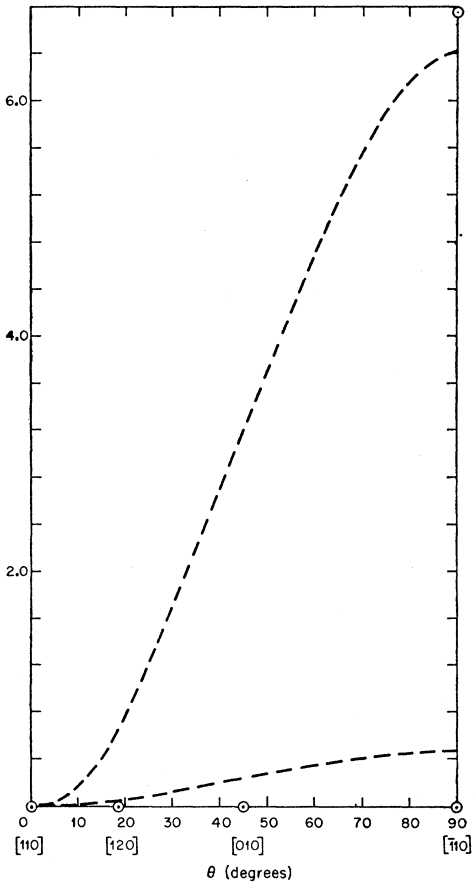


(c)

FIG. 11. Energy gain for $\mathbf{B}_{\bar{1}10}$, $\mathbf{E}$ rotated in (110) plane with longitudinal alignment. Compare with Fig. 9. (a) $b=0.1$. (b) $b=1.0$. (c) $b\rightarrow\infty$; - - - $K'=1$; $\odot$ circles for $K'\rightarrow\infty$.

## APPENDIX

The longitudinal alignment of **B** and **E** for the isotropic mass electron leads to the component equations

$$\begin{aligned} m\dot{v}_x &= qE_x + qv_yB, \\ m\dot{v}_y &= -qv_xB, \\ m\dot{v}_z &= qE_z, \end{aligned} \tag{A1}$$

where $B=B_z$. With initial requirements $v_x=v_y=v_z=0$ at $t=0$, one finds

$$\begin{aligned} v_x &= A\sin\omega t, \\ v_y &= -E_x/B(1-\cos\omega t), \\ v_z &= (q/m)E_zt, \end{aligned} \tag{A2}$$

and the related displacements

$$\begin{aligned} &x=\frac{A}{\omega}(1-\cos\omega t), \quad y=-\frac{E_x}{B}\left(t-\frac{1}{\omega}\sin\omega t\right), \\ &z=\tfrac{1}{2}(q/m)E_zt^2. \end{aligned} \tag{A3}$$

The constant $A$ is evaluated by direct substitution of (A2) into (A1) in similar fashion as was done in arriving at (14) for the nonscalar mass. Thus in evaluating the energy gain, the value of $A$ is $qE_x/m\omega=E_x/B$. The kinetic and potential energies are formally

$$\begin{aligned} W_{\text{K.E.}} &= \int_0^t m\dot{v}_x\frac{dx}{dt}dt+\int_0^t m\dot{v}_y\frac{dy}{dt}dt+\int_0^t m\dot{v}_z\frac{dz}{dt}dt, \\ W_{\text{pot}} &= \int_0^t qE_x\frac{dx}{dt}dt+\int_0^t qE_z\frac{dz}{dt}dt. \end{aligned} \tag{A4}$$

Explicitly, one obtains for the energy

$$W_{\text{pot}}=\left(\frac{E_x}{B}\right)^2 m(1-\cos\omega t)+\frac{1}{2}\frac{q^2E_z^2}{m}t^2=W_{\text{K.E.}}. \tag{A5}$$

The energy relation for the electrons in germanium is calculated similarly; but now, because of the tensor mass, cross products of the velocities enter and the algebra becomes quite cumbersome. The $W_{\text{pot}}$ now contains all three components of **E**, so via (9) and (11) one finds

$$\begin{aligned} W_{\text{pot}}=\int_0^t &\left\{-qE_y\frac{E_1}{qB}+qE_y\frac{E_1}{qB}\cos\omega t\right. \\ &\left.+\frac{qE_y}{\omega\mu}\sin\omega t[M_1E_2-M_2E_1]\right\}dt \\ +\int_0^t &\left\{qE_x\frac{E_2}{qB}-\frac{qE_xE_2}{qB}\cos\omega t\right. \\ &\left.+\frac{qE_x}{\omega\mu}\sin\omega t[M_4E_1-M_2E_2]\right\}dt \\ +\int_0^t &qE_z\left\{\frac{qE_zt}{m_{33}}-\frac{m_{31}}{m_{33}}\left[\frac{E_2}{qB}(1-\cos\omega t)\right.\right. \\ &\left.+\frac{\sin\omega t}{\omega\mu}(M_4E_1-M_2E_2)\right] \\ &-\frac{m_{32}}{m_{33}}\left[-\frac{E_1}{qB}(1-\cos\omega t)\right. \\ &\left.\left.\left.+\frac{\sin\omega t}{\omega\mu}(M_1E_2-M_2E_1)\right]\right\}dt. \end{aligned} \tag{A6}$$

The solution of (A6), after some manipulation, may be put into the form

$$\begin{aligned} W_{\text{pot}}=&\frac{1}{2}\frac{q^2E_z^2}{m_{33}}t^2+\frac{1}{B}\left(E_xE_2-E_yE_1\right. \\ &\left.-\frac{m_{31}}{m_{33}}E_zE_2+\frac{m_{32}}{m_{33}}E_zE_1\right)\left(1-\frac{1}{\omega}\sin\omega t\right) \\ &+\frac{q}{\omega^2\mu}\left\{E_y(M_1E_2-M_2E_1)+E_x(M_4E_1-M_2E_2)\right. \\ &\left.-E_z\left[\frac{m_{31}}{m_{33}}(M_4E_1-M_2E_2)+\frac{m_{32}}{m_{33}}(M_1E_2-M_2E_1)\right]\right\} \\ &\times(1-\cos\omega t), \end{aligned} \tag{A7}$$

which clearly reduces to (A5) in the scalar-mass limit. The $W_{\text{K.E.}}$ is formulated as

$$W_{\text{K.E.}}=\frac{1}{2}(M_1v_x^2+M_4v_y^2)+M_2v_xv_y+\frac{1}{2}\frac{q^2E_z^2}{m_{33}}t^2, \tag{A8}$$

whence one obtains the result

$$\begin{aligned} W_{\text{K.E.}}=&\frac{1}{2}\frac{q^2E_z^2}{m_{33}}t^2+\frac{1}{q^2B^2}(M_1E_2^2+M_4E_1^2-2M_2E_1E_2) \\ &\times(1-\cos\omega t). \end{aligned} \tag{A9}$$

The equivalence of $W_{\text{pot}}$ and $W_{\text{K.E.}}$ is readily apparent, if one considers the case $E_x=0$, $E_y=E\sin\theta$, $E_z=E\cos\theta$ with

$$\begin{aligned} E_1&=-(m_{13}/m_{33})qE\cos\theta, \\ E_2&=qE[\sin\theta-(m_{23}/m_{33})\cos\theta]; \end{aligned}$$

$W_{\text{pot}}$ reduces to (A9), and the nonperiodic term is precisely that used in (16) of the text.